International Journal of Bioprinting

RESEARCH ARTICLE

# PVDF/AgNP/MXene composites-based near-field electrospun fiber with enhanced piezoelectric performance for self-powered wearable sensors

**Cheng-Tang Pan[1,2†], Karishma Dutt[1†], Amit Kumar[3], Rahul Kumar[1], Cheng-Hsin Chuang[3], Yi-Ting Lo[4], Zhi-Hong Wen[5], Chien-Shu Wang[4*], Shiao-Wei Kuo[2,6,7*]**

[1]Department of Mechanical and Electro-Mechanical Engineering, National Sun Yat-sen University, Kaohsiung 80424, Taiwan

[2]Institute of Advanced Semiconductor Packaging and Testing, College of Semiconductor and Advanced Technology Research, National Sun Yat-sen University, Kaohsiung 80424, Taiwan

[3]Institute of Medical Science and Technology, National Sun Yat-sen University, Kaohsiung 80424, Taiwan

[4]Department of Psychiatry, Kaohsiung Armed Forces General Hospital, Kaohsiung, 80284, Taiwan, ROC

[5]Department of Marine Biotechnology and Resources, National Sun Yat-sen University, Kaohsiung 80424, Taiwan

[6]Department of Materials and Optoelectronic Science, Center for Functional Polymers and Supramolecular Materials, National Sun Yat-sen University, Kaohsiung 80424, Taiwan

[7]Department of Medicinal and Applied Chemistry, Kaohsiung Medical University, Kaohsiung 807, Taiwan

[†]These authors contributed equally to this work.

***Corresponding author:**
Shiao-Wei Kuo
(kuosw@faculty.nsysu.edu.tw)

**Citation:** Pan C-T, Dutt K, Kumar A, *et al*., 2023, PVDF/AgNP/MXene composites-based near-field electrospun fiber with enhanced piezoelectric performance for self-powered wearable sensors. *Int J Bioprint*, 9(1): 647. https://doi.org/10.18063/ijb.v9i1.647

**Received:** June 24, 2022
**Accepted:** September 11, 2022
**Published Online:** November 24, 2022



(This article belongs to the *Special Issue: Near-field Electrospinning and Melt Electrowriting for Biotechnology and Biomedicine*)

## Abstract

MXenes, as highly electronegative and conductive two-dimensional nanomaterials, are extensively studied for their use in sensors and flexible electronics. In this study, near-field electrospinning was used to prepare a new poly(vinylidene difluoride) (PVDF)/Ag nanoparticle (AgNP)/MXene composite nanofiber film as a self-powered flexible human motion-sensing device. The composite film displayed highly piezoelectric properties with the presence of MXene. Scanning electron microscopy, X-ray diffraction, and Fourier transform infrared spectroscopy revealed that the intercalated MXene in the composite nanofibers was evenly spread out, which not only prevented the aggregation of MXene but also enabled the composite materials to form self-reduced AgNPs. The prepared PVDF/AgNP/MXene fibers displayed exceptional stability and excellent output performance, enabling their use for energy harvesting and powering light-emitting diodes. The doping of MXene/AgNPs increased the electrical conductivity of the PVDF material, improved its piezoelectric properties, and enhanced the piezoelectric constant of PVDF piezoelectric fibers, thereby allowing the production of flexible, sustainable, wearable, and self-powered electrical devices.

***Keywords*:** Near-field electrospinning; Piezoelectric fibers; Sensing elements; Conductive fillers; Composite materials

## 1. Introduction

The internet of things (IoT) will benefit from the ubiquitous use of sensor networks in our daily lives, such that each person and everything will be connected. Wearable electronics, for example, can be positioned on skin, clothes, or accessories, allowing users to monitor and receive feedback on their health and physical activities[1–3]. While being an essential aspect of the IoT, these devices would likely function as personal assistants[4–8]. Wearable electronics should be light in weight, inexpensive, small, flexible, and sustainably powered[9]. These requirements cannot be met by existing batteries, as they are too bulky and have relatively short lifespan. Nevertheless, various pressure sensors, including resistive, capacitive, piezoresistive, and piezoelectric sensors, are available in the market[10–12]. In most cases, the output of these sensors is an electrical signal that varies depending on the amount of force or pressure applied[13–15]. Practical sensing applications require not only the conversion of mechanical signals into electrical signals but also an instantaneous, linear, and stable response. It is generally difficult to achieve an instantaneous, linear, and stable response with piezoresistive pressure sensors; moreover, in the interest of energy and environmental sustainability, renewable energy sources should ideally be used to power such devices. Piezoelectric materials have been extensively researched on in recent years for their capacity to transform mechanical energy into electrical energy, and vice versa. In particular, there has been a great deal of interest in the use of organic piezoelectric materials for fabricating flexible and wearable electronics due to their low density, high sensitivity, biocompatibility, stretchability, wide detection range, low to zero power consumption, high output, rapid response, flexibility, and ease of processing[16–20].

Piezoelectricity is a phenomenon of electromechanical conversion between mechanical and electrical energy. Although non-centrosymmetric material is not a sufficient requirement, it is necessary to display this effect[21–24]. With the exception of cubic class 432, all non-centrosymmetric crystallographic classes display piezoelectricity[25]. Pierre and Jacques Curie were the first to discover that the asymmetric movement of ions or charges in piezoelectric materials is caused by deformation via the changes in electrical polarization[26–28]. Due to their relatively high piezoelectric coefficients and natural flexibility, poly(vinylidene fluoride) (PVDF) and its copolymers have been widely used in the production of organic piezoelectric materials[29–32]. Kawai *et al.* discovered that PVDF has five main phases: alpha (α), beta (β), gamma (γ), epsilon (ε), and delta (δ)[32]. The main electroactivity of PVDF arises from its crystalline ferroelectric phases (γ- and β-phase), with the γ-phase being less electroactive than the β-phase[33]. Since the piezoelectric coefficients of PVDF materials are substantially lower than those of piezoelectric ceramics, PVDF materials have not been employed as self-powered sensors in actual applications. In order to enhance the piezoelectric capabilities of PVDF and its copolymers, two techniques have been employed: increasing the piezoelectric phase content and enhancing the residual polarization[34]. It is generally difficult to achieve a high content of the β-phase through solution processing and conventional melting[35], but there are several strategies to do so, including incorporating fillers[36], mechanical stretching, heat treatment, and polarizing[37,38]. Electrospinning has been recognized as a feasible approach to converting the non-electroactive phase into the electroactive phase (γ- and β-phase). The electrospinning of a PVDF solution allows the conversion of the nonpolar α-phase into the polar β-phase.

Near- and far-field electrospinning can be used to enhance the piezoelectric characteristics of PVDF. Electrospinning, as an excellent approach for fabricating polymer fibers, was first patented in the United States in 1902[39]. Until the 1990s, this technique was often neglected, but it re-emerged as a leading technique following the rapid development and applications of nanofibers. It is possible to control the diameters and morphologies of electrospun fibers by modifying the process parameters, particularly the molecular weight, solution properties (*e.g.*, surface tension, conductivity, and viscosity), flow rate, electric voltage, and distance between the needle and the collection plate. In this study, the parameters of near-field electrospinning (NFES) [40–42] were optimized to develop flexible, dynamic, and soft sensing elements of PVDF piezoelectric fibers incorporating silver nanoparticles (AgNPs) and transition metal carbide/nitride (MXene). NFES was performed in conjunction with a rolling collection system and its *XY*-axis digital control platform. In order to optimize the piezoelectric fibers, the needle and rotating collector were vertically aligned to collect the fibers produced by electrospinning. The stainless-steel needle was connected to a positive high-voltage source. Under the effects of gravity, the vertical collection method makes it easy to break through the spinneret to collector surface. With the software-controlled platform moving back and forth, continuous piezoelectric fibers were obtained through electrospinning. Through the combined effects of the conductivity, viscosity, and contact angle of the best precursor solution, a Taylor cone was formed, when the electrostatic force, provided by the electric field, was greater than the droplet surface tension, resulting in a large amount of orderly material collected on the rotating collector with parallel electrospinning[43–46].

Transparent electrodes, which are often used for organic light-emitting diodes (OLEDs)[47], touch screens, and thin-film silicon solar cells, have thrived along with the advancements in smartphone technology[48]. Although indium tin oxide (ITO)[49] has been the predominant material in transparent electrodes, it is a brittle material that requires a vacuum environment for production, making its thin-film fabrication process costly and energy-consuming. Furthermore, the limited interfacial area between the molecular chains of PVDF and typical conductive fillers poses a challenge to achieving adequate filler–dipole interactions and increasing dipole polarization during the electrospinning of piezoelectric PVDF or its copolymers. The incorporation of conductive fillers into polymer solutions has the potential to increase the intensity of the electric field, thus resulting in an increase in the polarization of polymer dipoles at a constant voltage[50–53]. Several conductive active nanofillers have been employed to build conductive networks on various substrates, such as graphene (rGO)[54], carbon nanotubes (CNTs)[55], AgNPs[56], MXene[57], and silver nanowires (AgNWs)[58], showing excellent conductivity and transmissivity; all of which have been developed as alternatives to ITO[59,60]. The use of nanocomposites strategy, with an emphasis on the inclusion of conductive nanofillers, represented by graphene and carbon nanotubes[53,61], is a direct approach to improving piezoelectricity, and therefore the sensitivity of PVDF. By using a small amount of conductive nanofillers, it is possible to increase the piezoelectric phase development, produce strong interfacial coupling effects, and preserve the high flexibility of PVDF, all of which are useful for increasing the sensitivity of nanocomposites.

Silver is an attractive material on account of its antibacterial properties, electrical conductivity, and relatively low cost. Although AgNPs have enormous surface areas that are rich in electrons, their vulnerability to oxygen ($O_2$) prevents them from being employed directly. A biocompatible and reducible PVDF has been created to prevent the oxidation of AgNPs and enhance their electrical stability[62,63]. Furthermore, AgNPs have been widely used as fillers in polymer matrices in view of their excellent ability to improve the crystal β-phase structure of PVDF[64,65]. A β-phase content of approximately 80% can be achieved with the addition of AgNPs to PVDF. The interaction between electron-rich AgNPs and the F atoms in PVDF increases the piezoelectricity and the β-phase content, resulting in electrically conductive particles in nanofibers upon electrospinning, and thereby improving polarization[62,65–69].

MXenes are novel two-dimensional (2D) materials displaying excellent aqueous dispersion and electrical conductivity as well as abundant surface functional groups. MXenes have garnered widespread attention due to their distinctive electrical and mechanical characteristics, which make them ideal for supercapacitors, lithium-ion (Li-ion) batteries[70,71], and use in various applications[72], including strain sensors, energy storage[73,74], catalysis[75], electromagnetic interference (EMI) shielding[76], and healthcare[76–78]. MXene is an attractive alternative for nanocomposites engineering due to its nanometer-scale dimensions, huge aspect ratio, and great electric conductivity. While the majority of published works have focused on improving dielectric, electrochemical, and thermoelectric characteristics, a number of studies have looked into MXene's capacity to modulate the piezoelectric capabilities of piezoelectric polymers because of its exceptional conductivity, layer structure, and active surface. Nevertheless, it is important to select an appropriate matrix to achieve high levels of flexibility, porosity, and permeability. Research has revealed that combining an MXene with PVDF would result in a composite with high permittivity and compatibility. Since conductive fillers and a high dielectric constant can improve the piezoelectric properties of a polymer, it is anticipated that MXenes would be excellent materials for increasing the piezoelectric capabilities of PVDF and its copolymers[79–81]. MXene can promote the formation of the piezoelectric phase, bring about a high interfacial coupling effect, and provide an improved piezoelectric response in PVDF, much like the conductive reinforcements, represented by graphene and carbon nanotubes. Additionally, it should be highlighted that MXene nanosheets have a stronger reinforcing effect than graphene and carbon nanotubes at the same loading amount. For instance, the maximum reported piezoelectric coefficient $d_{33}$ of MXene/PVDF hybrid film is 43 pC/N, compared to that of carbon nanotubes/PVDF, which is 23 pC/N. Meanwhile, it has been discovered that the presence of MXene nanosheet improves the mechanical performance, *i.e.*, the young's modulus, of PVDF. MXene/PVDF hybrid films have a greater voltage sensitivity Sv of up to 0.0480 V/N in detecting force when compared to traditional PVDF-based force sensors (Sv = 0.0221 V/N) due to their outstanding piezoelectric response and high Young's modulus[82].

The intercalated MXene in composite nanofibers is spread out evenly, which not only solves the problem of MXene aggregation but also enables the composite materials to self-reduce AgNPs *in situ*. More importantly, wearable electronics incorporating MXene/AgNP composites have significant EMI shielding properties, allowing them to protect the human body from potentially dangerous electromagnetic radiation. A new generation of multipurpose wearable electronic devices based on MXene/AgNP materials is expected to be launched[83–86].

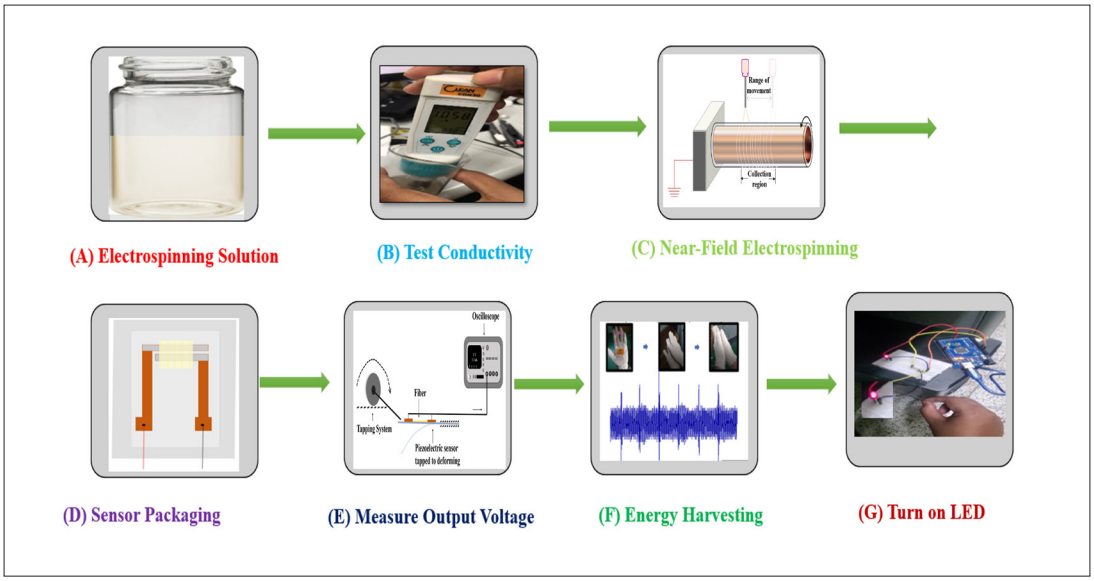


**Scheme 1**. Experiment process for fabricating PVDF/AgNP/MXene composite fibers through NFES: (A) Electrospinning the solution, (B) Testing the conductivity, (C) NFES, (D) Packing the sensor, (E) Measuring the output voltage, (F) Harvesting energy, and (G) Turning on an LED.

The porous structures and high specific surface areas of electrospun PVDF composite fibrous films engender them as ideal substrates for producing low-cost films[87,88].

In this study, we prepared new types of PVDF/AgNP/MXene composite nanofibers (Scheme 1A–C), characterized them using various techniques (Fourier transform infrared [FTIR] spectroscopy, X-ray diffraction [XRD], scanning electron microscopy [SEM], and piezoelectric measurements), and employed them in self-powered wearable devices (Scheme 1D and E). These composite fiber materials displayed extremely high conductivity as well as good mechanical and piezoelectric capabilities. The integration of AgNP/MXene composites into the PVDF matrix developed the electroactive β-phase and improved the piezoelectric properties of PVDF. These are potentially advantageous for future self-powered flexible and wearable optoelectronic devices. We encapsulated interdigitated electrodes (IDEs), comprising copper (Cu), PVDF/AgNP/MXene piezoelectric fibers, and flexible poly(ethylene terephthalate) (PET) substrates, into poly(dimethyl siloxane) (PDMS). These piezoelectric devices were packaged in PDMS to enhance their durability (Scheme 1F). We achieved a high-voltage output from the PVDF/AgNP/MXene piezoelectric fibers with the desired morphology, thus enabling them to turn on an LED (Scheme 1G).

## 2. Materials and methods

### 2.1. Synthesis of MXene

MXene ($Ti_3C_2$) was synthesized by eliminating an intermediary element (Al atoms) from the MAX phase ($Ti_3AlC_2$) using minimally intensive layer delamination (MILD) etching. Commercial lithium fluoride (LiF) powder (2 g) was dissolved in concentrated hydrochloride (HCl; 9 M, 30 mL) and deionized (DI) water (10 mL), and continuously magnetically stirred (300 rpm) at room temperature for 10 mins. $Ti_3AlC_2$ powder was added slowly and carefully, and the mixture was continuously stirred (300 rpm) at 35°C for 36 h. The resultant suspension was centrifuged (5 min per cycle) with DI water (3500 rpm), and then decanted until the pH of the supernatant neared 6. At the end of the process, the products were washed with ethanol and dried overnight under vacuum at 60°C to obtain a stable liquid-free delaminated MXene in powdered form. The overall process is illustrated in Figure 1A.

### 2.2. AgNP/Mxene hybrid composites

MXene was dispersed in DMSO. The mixture was sonicated for at least 30 min to break up any agglomerates and was then magnetically stirred at 250 rpm for 30 min on a heater. $AgNO_3$ (content kept at 10 wt% relative to the weight of MXene) was introduced into the suspension. After sonication for another 30 min, the solution appeared black, and the mixture was stirred magnetically for 30 min.

### 2.3. Conductivity measurements

In order to measure the conductivity, a clean CON30 conductivity meter was used.

### 2.4. Morphological characterization

The surface morphology of the synthesized $Ti_3C_2$ MXene was examined under ultrahigh resolution using transmission electron microscopy (TEM); its selected area electron diffraction (SAED) patterns were also obtained.

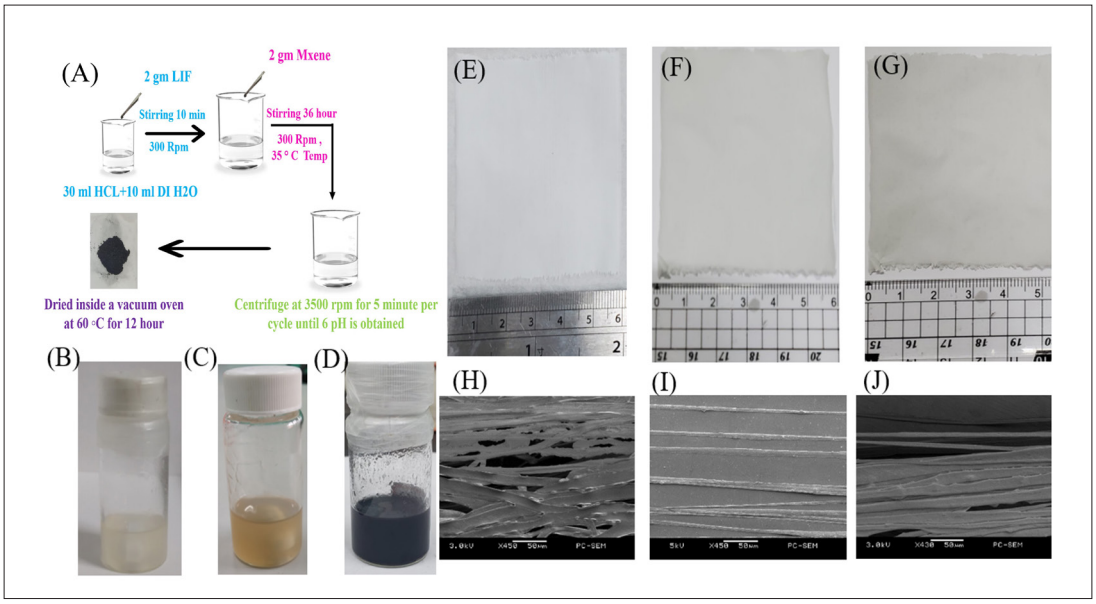


**Figure 1**. (A) Schematic representation of the synthesis of MXene. Electrospinning solutions of (B) pure PVDF, as well as (C) PVDF/AgNP and (D) PVDF/AgNP/MXene composites. Digital images of (E) pure PVDF, (F) PVDF/MXene, and (G) PVDF/AgNP/MXene fiber sheets. SEM images of (H) PVDF/MXene and (I, J) PVDF/MXene/AgNP fibers.

The JEOL JSM-6380 scanning electron microscope was used to analyze the surface appearance of the PVDF piezoelectric fibers and the PVDF/Mxene and PVDF/AgNP/MXene composite fibers.

### 2.5. Electrospun polymer fiber membrane

The electrospinning solutions were prepared as shown in Figure 1B–D. The PVDF (Figure 1B) and PVDF/AgNP (Figure 1C) solutions were prepared using a previously reported procedure[89,90]. The optimal operating parameters were as follows: a PVDF content of 18 wt%, a direct-current (DC) voltage of 14 kV, and a tube rotation velocity of 1900 rpm. The PVDF powder was dissolved in acetone and DMSO (1:1, v/v). In order to prepare the PVDF/AgNP/MXene (Figure 1D) composite fiber membrane, PVDF (18 %wt) was dissolved in acetone, and the desired amounts of MXene-AgNP/DMSO suspensions were added, respectively, under magnetic stirring; the mixtures were stirred for 12 h at room temperature in an airtight container to form homogeneous solutions. As illustrated in Figure 1C and D, the AgNP/DMSO and AgNP-MXene/DMSO solutions appeared pale-yellow and black, respectively. A research laboratory-scale NFES apparatus was employed, comprising a positive power supply (0–40 kV), a negative high-power supply, a precision flow infusion pump, a needle, a rotating collection device, and a dual-axis platform controller. Scheme 2A is a schematic representation of the NFES device; its three primary elements were a metal spinning needle, a metal collector with reverse polarity, and a high-voltage power source (Scheme 2B). NEFS was performed by loading the prepared solution into a syringe with a stainless-steel needle tip. The propelling syringe was filled with the configured polymer solution and attached to the precision flow propulsion pump. The stainless-steel needle was connected to a power supply with high-voltage electric field (positive electrode) to function as the NFES nozzle. The grounding end was a glass tube (outer diameter: 20 mm; thickness: 0.50 mm) that contained the piezoelectric fibers, a direct current (DC) motor, and a negative high-voltage power supply (negative). Copper tape (thickness: ca. 0.10 mm) was wrapped around the glass tube to ensure that the electric field makes contact with the ground (negative electrode). When a high voltage was applied to the needle, an electric field was formed between the spinning needle and the collector, resulting in the continuous spinning of the needle. The moving platform was controlled by a computer to move the needle laterally to collect the orderly and non-small area fibers with a specific stretching direction. Fibrous membranes were collected using a grounded, revolving collector. The fibers were dried at room temperature overnight.

### 2.6. Mechanical properties

The mechanical properties of the PVDF/AgNP/MXene composites were evaluated using a universal testing equipment (AGS-50KNXD, Shimadzu, Japan).

### 2.7. Sensor package and electrical characteristic measurement

#### *2.7.1. Fabrication of a wearable sensor*

This study investigates the complex piezoelectric responses of PVDF and PVDF-based composite fiber

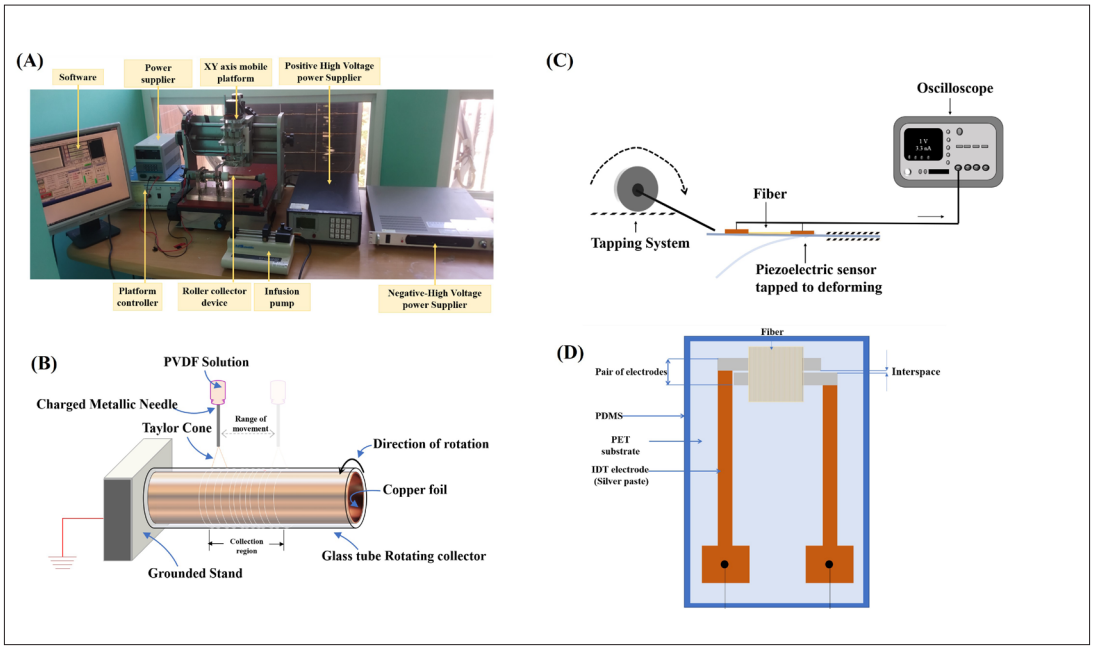


**Scheme 2**. (A) NFES equipment setup, (B) Schematic representation of NFES, (C) Equipment for the electrical measurement of voltage, and (D) A fabricated piezoelectric sensor.

structure. Firstly, the piezoelectric fiber and conductive copper tape were cut into the desired dimensions, and Ag paste was applied on the copper electrodes and conductive silver-plated wires in it, which served as the negative and positive electrodes of the piezoelectric device. Piezoelectric fiber sheets with a width of 10 mm were placed on a piece of a parallel copper interdigital electrode (IDE). Subsequently, flexible PET was tightly bonded to the IDE to achieve a large displacement, and the sensor was packaged with PDMS on both sides. Approximately 1,400 fibers were used, and PDMS was used as the package's outmost material to create a flexible sensor. Then, the PET with the Ag glue applied on the copper electrodes and silver-plated wire in it was placed in a vacuum ball to extract the vacuum, as shown in Scheme 2D. This step involves removing the bubbles created during the vacuum process and heating them for 15 min on the heating plate.

### *2.7.2. Electrical measuring instrument*

After that, the fiber was encapsulated by PDMS and attached to the electrical measurement device. The sensor was distorted instantly by tapping it with a rotating beater. The GW Instek GDS-2104A oscilloscope was used to measure the electrical properties. The piezoelectric sensor was deformed to perform a reliability test. The deformation of the piezoelectric fiber generated the voltage data. As the voltage measured in the experiment was easily interfered by noise, such as impact and flapping, when performing the voltage measurement experiment, it was necessary to measure the positive and negative poles, respectively, to prove that the measured signal was piezoelectric. When the polarization direction changed the shape of the piezoelectric fibers, the electrons inside the material were pushed out and became free electrons. The piezoelectric $d_{33}$ mode turned the mechanical strains that were spread along the fibers into an alternating voltage; this procedure is illustrated in Scheme 2C. In the design of piezoelectric energy harvesting, piezoelectric coefficient $d_{33}$ may be used as a parameter to determine the appropriate piezoelectric material. Only piezoelectric coefficient $d_{33}$ needs to be tested in the experiment. The short-circuit charge collected on the electrodes of piezoelectric energy harvesting per unit applied mechanical stress is the physical meaning of d, indicating that the greater the d, the larger the possible charge collected in the short circuit.

There are several methods for determining the $d_{33}$ coefficient of piezoelectric materials, including utilizing a $d_{33}$ meter[82] and a pneumatic pressure rig[91]. It would be straightforward and simple to characterize PVDF with a $d_{33}$ meter, but it has been reported that $d_{33}$ meters may not provide the most accurate readings on thin films or very thin samples[92]. $d_{33}$ must be tested according to the formulation of mathematical equations[93]. Since there is no direct apparatus to measure $d_{33}$, a comparative technique was adopted, and a representative PVDF material with an identical $d_{33}$ value was created for reference[82].

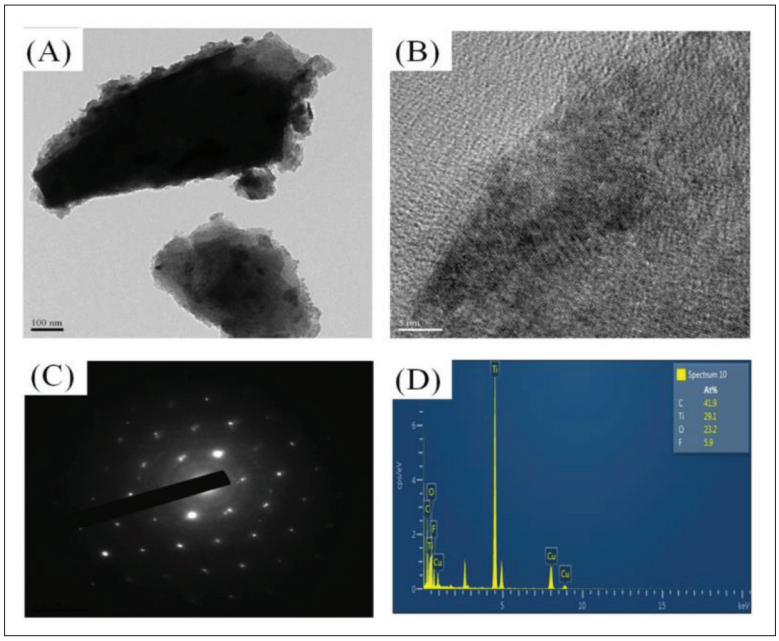


**Figure 2**. (A) Low-magnification TEM image of the 2D MXene $Ti_3C_2$, (B) High-magnification TEM image of the synthesized stacked layers of the bulk Mxene, (C) SAED pattern, and (D) EDS spectrum and atomic percentages of the residue of $Ti_3C_2$ MXene.

## 3. Results and discussion

### 3.1. MXene

The as-synthesized MXene $Ti_3C_2$ powder was characterized using TEM, SAED patterns, and energy dispersive spectrometry (EDS). Figure 2A and B presents low- and high-magnification TEM images, revealing the flake-like appearance of nanosheets following exfoliation, along with apparent layered structures of the MXene material. The associated SAED pattern (Figure 2C) reveals the hexagonal symmetry of the carbide layers, inherited from $Ti_3AlC_2$. The EDS spectrum in Figure 2D shows the atomic percentages of the residue of $Ti_3C_2$ MXene; a large proportion of the char residue featured the anatase phase of $Ti_3C_2$, with O and F atoms represented in comparatively small proportions (ca. 23.2% and 5.9%, respectively).

### 3.2. PVDF/Ag-NP/MXene electrospun fibers

We prepared PET-based piezoelectric devices, featuring new PVDF/AgNP/MXene electrospun fibers, and compared the behavior of electrospun fibers formed from PVDF, PVDF/AgNP, PVDF/Mxene, and PVDF/AgNP/MXene. The decoration of Ag atoms on the MXene sheets was achieved through $AgNO_3$ self-reduction, as demonstrated using morphological, functional, and structural characterizations. Figure 1 displays the fabrication process of the all-fiber structures. Doping stretchable polymer fibers with high-conductivity NPs allowed the development of novel functionality, including the ability to detect physical deformations. Since its metallic conductivity is better than those of other solution-processed nanomaterials, 2D titanium carbide MXene is a promising material for producing conducting and stretchy fibers. MXenes are a broad classification of 2D materials that have extraordinarily high electrical conductivity (up to $10^4$ S/cm). We assumed that the inclusion of this MXene would improve the conductivity of the polymer solution; thus, in order to develop fibers that have a unique mix of electrical conductivity and stretchability, a better understanding is required of the interactions between MXene and the polymer material. In a previous study, we found that an 18 wt% PVDF solution had the desired viscosity and surface tension for NFES[94]; hence, we measured the conductivity of composites prepared from 18 wt% PVDF and AgNP/MXene. Here, we found that the electrical conductivity increased from 40 to 1,148 μS/cm following the addition of MXene/AgNP composite to PVDF solution, primarily because the inclusion of AgNPs in MXene improved the electrical conductivity of PVDF composites.

In order to study the influence of the solution concentration, the NFES process parameters were adjusted as follows: a 20 G needle (outer diameter: 0.91 mm; inner diameter: 0.61 mm), the speed of the *XY* dual-axis digital control platform at 2 mm/s, a high-voltage input of the needle at 14 kV, molecular weight, and the distance between the needle and the roller collection device at 1 mm. The nanofibers prepared from PVDF/AgNP/MXene with long-lasting piezoelectricity were directly etched on the glass tube. Figure 1E–G presents the images of pure PVDF,

PVDF/MXene, and PVDF/AgNP/MXene fiber sheets, respectively; as expected, the color varied from white to blackish upon increasing the concentration of MXene.

We used SEM to investigate the morphologies of MXene composite fibers in greater detail. A well-aligned fiber at the contact would favor the production of well-oriented β-form extended-chain crystallites at the interface. The diameters of the fibers were determined from SEM images recorded at four different locations along their length. The electrospinning of MXene composite fibers resulted in fibers that were perfectly aligned with one another. Although the PVDF/AgNP/MXene fibers were continuous and had porous network topologies, there was no beading throughout the fibers. Figure 1H–J shows high-magnification SEM images of PVDF/MXene/AgNP composite fibers. Thinner fibers were formed in the presence of MXene, most likely because of the increased static electrical field caused by the higher solution conductivity. There were a few minor bumps, resulting in unsmooth fibers, as well as micron-sized MXene, which resulted in slightly uneven fiber diameters; the PVDF/MXene fiber diameters ranged from 0.39 to 4.50 μm (Figure 1I). With the addition of AgNP, the fibers became clear and dry, presumably because the AgNPs enhanced the thermal conduction, thereby enhancing solvent evaporation during the fly process in the electrical field and following the deposition on the rotating disk. The diameters of the PVDF/AgNP/MXene fibers ranged from 1.0 to 6.5 μm (Figure 1J). Nevertheless, the fiber surfaces had uneven structures (surface roughness and bumps), presumably due to regionally nonuniform MXene distributions produced by slower solvent evaporation, as a result of interactions between the hydrophilic MXene and the humid atmosphere (Figure 1H).

We used FTIR spectroscopy and XRD to determine the chemical and crystalline structures of the materials used in this study. Figure 3A presents the FTIR spectra of MXene, AgNPs, and PVDF in range from 1,700 to 750 $cm^{-1}$. Signals at 840, 1,071, 1,275, and 1,402 $cm^{-1}$ are typical of the β-phase. After the addition of MXene, the β-phase became more apparent, and the width became narrower. The sample containing AgNPs had the highest content of the β-phase. Signals for Ti–O, C–O, and C–F bonds in the MXene were also evident. The signal for Ti–O bonds moved from 1,624 to 1,644 $cm^{-1}$, revealing that the C–F bonds of PVDF and the surface groups of MXene interacted through dipole–dipole interactions.

The (002) diffraction peak of MXene was evident in the XRD patterns of PVDF/AgNP/MXene fiber films. In addition, the signals for the (111), (200), (221), and (311) planes of the Ag crystal were all present at values of 2θ of

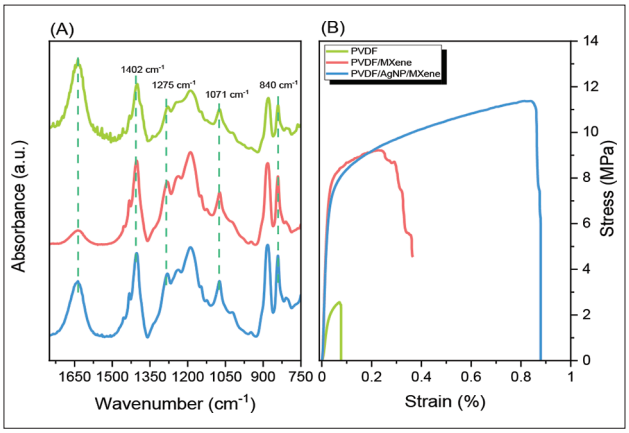


**Figure 3**. (A) FTIR spectra of pure PVDF, PVDF/MXene, and PVDF/AgNP/MXene composite materials and (B) their corresponding tensile stress-strain curves.

38.14, 44.4, 64.4, and 77.6°, respectively (Figure 4A). The usual (110) diffraction peak of α-phase PVDF, appearing at a value of 2θ of 20.2°, became less prominent following the increase in concentration of MXene in the films. Similarly, the (021) diffraction peak of β-phase PVDF appeared at a value of 2θ of 20.8°. These changes in crystalline form suggested that the PVDF chains were nucleated by MXene in a very heterogeneous manner and indirectly confirmed that there were strong interactions at the interface between MXene/AgNP and PVDF.

When mechanical forces are applied to piezoelectric materials, they deform and change their polarization density almost instantly. This behavior causes a voltage to appear in the polar direction, and vice versa. The composite products exhibited an outstanding mechanical performance, owing to strengthening mechanisms. The practical applications of composite materials are limited by poor mechanical properties. Therefore, the mechanical properties of piezoelectric materials are crucial factors when attempting to increase the piezoelectric response. However, they are often overlooked when engineering piezoelectric materials. Although Young's modulus has been studied in relation to the piezoelectric characteristics of piezoelectric polymers, there is still a need to investigate the effects of other mechanical qualities, including compression modulus and flexibility[83,95-97]. Polymer composite materials are not useful if they have poor mechanical qualities[51–53]. Therefore, the mechanical characteristics of PVDF as well as PVDF/MXene and PVDF/AgNP/MXene composites were investigated (Figure 3B). As observed in our experiments, the AgNP-and-MXene-based piezoelectric fiber displayed superior mechanical characteristics. The mechanical properties of the two types of fillers were different due to their varying volume fractions. The following observation demonstrated

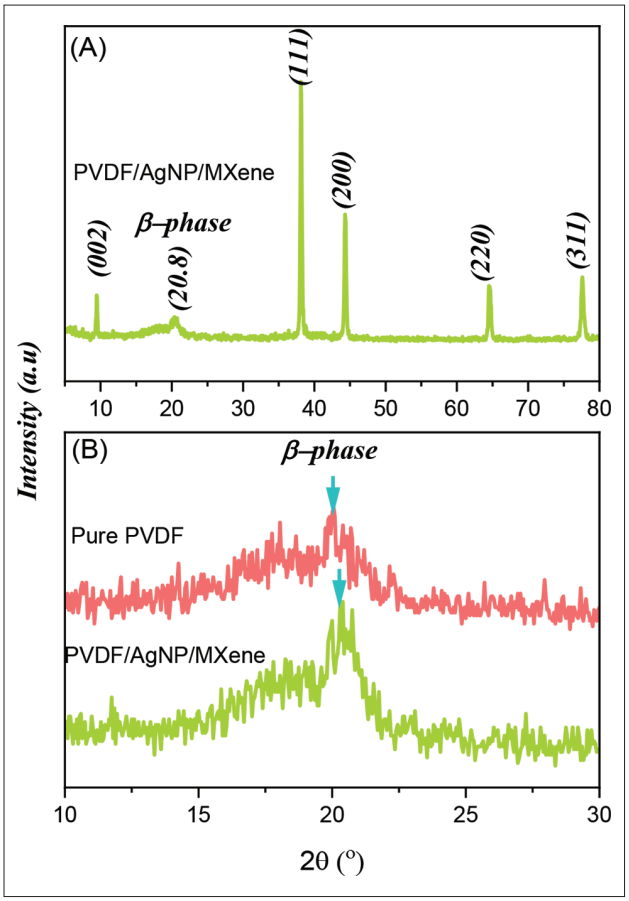


**Figure 4**. XRD patterns of (A) PVDF/AgNP/MXene composite membrane as well as, (B) pure PVDF and PVDF/AgNP/MXene composite membranes.

that the quasi AgNPs and MXene worked together to improve the mechanical qualities: tensile strength of PVDF/MXene/AgNP > tensile strength of PVDF/Mxene > tensile strength of PVDF. The maximum tensile stress improved from approximately 2.0 to 10.5 MPa in the presence of 5 wt% MXene, as a result of the interactions between the polymer chains and the MXene with AgNPs, thereby strengthening the electrospun fibers. Notably, incorporating MXene into AgNP/PVDF fibers led to much greater strain to failure and strength, relative to those of pure PVDF fibers. The toughness was a measure of the nanofibers' stretchability. Indeed, the stress–strain curves of the PVDF/AgNP/MXene composite fiber revealed increased toughness. Compared with pure PVDF fibers, the mechanical properties of PVDF fibers incorporating AgNPs and MXene were effectively enhanced. In particular, when compared with pure PVDF and PVDF/AgNP composit fibers, the tensile strength, young's modulus, and toughness of the PVDF/AgNP/MXene fiber film were superior, verifying the synergistic impact of PVDF, AgNPs, and MXenes on the mechanical characteristics of the fibers, as shown in **Table S1**.

### 3.3. Piezoelectric characteristics of PVDF/AgNP/MXene composite membrane

Our objective for this study was to achieve a high-voltage output from PVDF/AgNP/MXene piezoelectric fibers. Prior to analyzing the piezoelectric properties of the fibers, we confirmed the piezoelectric effect. The data from the positive and negative two-pole positive and reverse electrical measurement devices showed opposing peaks, as seen in Figure 5.

The electrical tapping tests (Figure 6) confirmed that the output voltage of the PVDF/AgNP/MXene composite piezoelectric fiber was significantly higher than that of pure PVDF as well as PVDF/AgNP and PVDF/MXene composites. Therefore, doping the PVDF piezoelectric fiber with AgNP/MXene would increase the voltage. The piezoelectric property is dominated by the young's modulus and piezoelectric coefficient of piezoelectric materials. Piezoelectric materials would achieve higher piezoelectric performance with a larger piezoelectric coefficient and a smaller young's modulus. The ability of piezoelectric materials to withstand changes in length would significantly affect the piezoelectric property[98]. In contrast to the substantial study and application of PVDF piezoelectric films, the present research on PVDF piezoelectric fibers is limited. In 2010, Pu *et al.* reported that the piezoelectric strain coefficient $d_{33}$ of PVDF piezoelectric fiber was 57.6 pm/V, while the that of commercially available PVDF piezoelectric film was 25 pm/V[99]. In this study, we used a unique technique to create piezoelectric PVDF composite films with much higher $d_{33}$ values than previously reported values. The piezoelectric coefficient ($d_{33}$) of the PVDF/AgNP/Mxene sample was verified, in which the $d_{33}$ value was found to be 52.23 pC/N. The results are given in **Table S2** for a better comparison. Tapping tests were also conducted to evaluate the sensitivity of the fabricated pressure sensor based on the PVDF/AgNP/MXene hybrid fiber film. **Figure S1** shows that the output voltage was tested at several low frequencies ranging from 1, 2, 3, 4, 5, and 7 Hz. Sensors based on PVDF/AgNP/MXene are sensitive to variations in the applied frequency. The voltage response of the sensor based on PVDF/AgNP/MXene, as shown in **Figure S1**, increases with increasing frequency, with a maximum voltage sensitivity of 0.31428 V $Hz^{-1}$, which is larger than the that of PVDF/MXene (0.242 V $Hz^{-1}$) and PVDF (0.010 V $Hz^{-1}$) sensors[44]. High stability and reliability are also necessary for the practical deployment of flexible force sensors. A cantilever vibration test was conducted to assess the operating stability and reliability

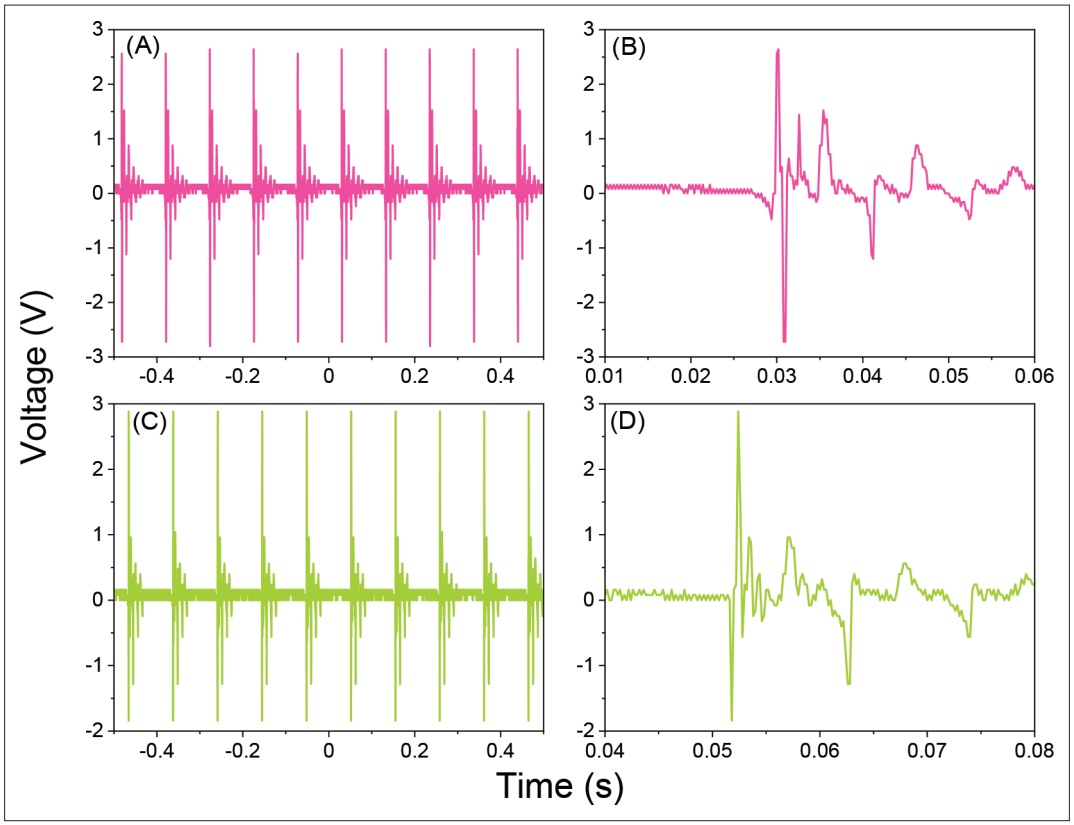


**Figure 5**. Piezoelectric properties and voltage output of the PVDF/AgNP/MXene composite: (A, B) forward and (C, D) reverse connections.

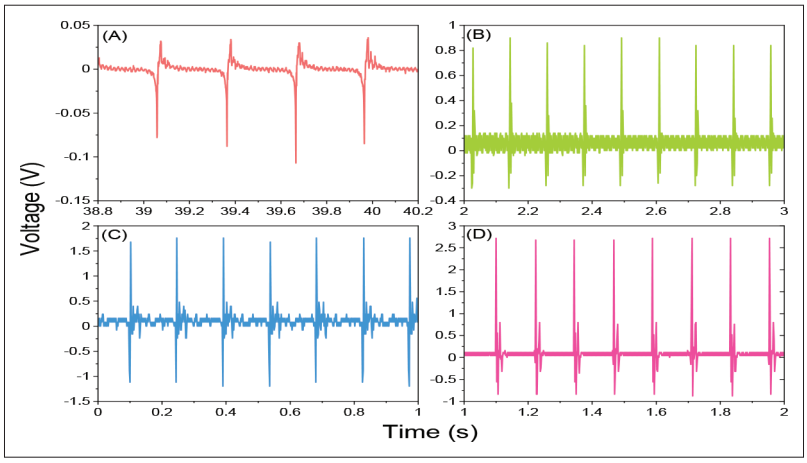


**Figure 6**. Piezoelectric response of (A) pure PVDF, (B) PVDF/AgNP, (C) PVDF/MXene, and (D) PVDF/AgNP/MXene.

of the sensor, in which the schematic representation of the test is shown in Scheme 2C. **Figure S2** shows the output response of the PVDF/AgNP/Mxene hybrid sensor at 1 Hz driving frequency. The sensors exhibit superior stability and durability as long-term effective and durable sensors as they can run consistently for over 1 week (one cycle of 1,000 s per day) without performance deterioration.

We investigated the potential of using PVDF/AgNP/MXene composite fiber as a self-powered wearable sensor for the detection of human motion, with regard to the exceptional flexibility and energy-harvesting capabilities of the device. Figure 7 shows the voltage outputs of the sensor detecting the clapping of hands, moving of arms, moving of fingers, and walking.

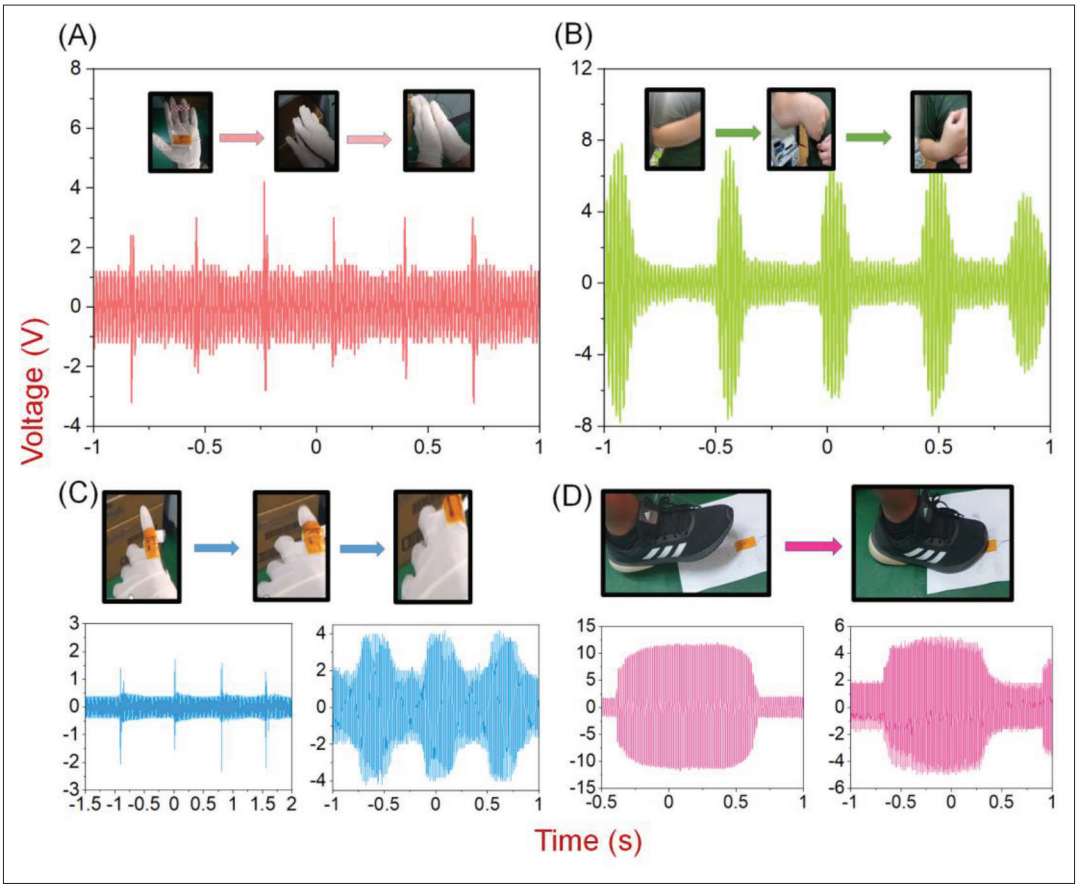


**Figure 7**. Applications of PVDF/MXene/AgNP composite as a self-powered sensor for the detection of human motion. Voltage outputs of the sensor detecting the (A) clapping of hands, (B) moving of arms, (C) moving of fingers, and (D) walking.

The gloves were first attached with fabricated nanofiber mats, and the voltage output was then monitored when clapping hands, thereby converting hand pressure into electricity (Figure 7A). The voltage output was measured when clapping hands at different frequencies. Figure 8 reveals that the consecutive clapping of hands resulted in voltage responses that were recoverable and steady. More notably, when a person clapped his or her hands, first slowly, and then quickly, the output voltage frequency reacted in a manner consistent with the movement, indicating good synchronization. Subsequently, sensors were connected to the underarm of clothing and to the medial elbow (Figure 7B). The sensors detected the movement of the arms and converted the arm pressure into electricity, resulting in a series of voltage signals. When we attached the sensor to a finger, it detected finger movements, converting finger pressure into electricity (Figure 7C). In addition, walking was detected by a sensor attached to the ground, converting leg pressure into electricity (Figure 7D). The output voltages provided repeatable, steady, and synchronous signals.

The presence of AgNP/MXene composite in PVDF also enhanced the electrical conductivity of the material, thereby improving the piezoelectric characteristics of the whole fiber. The output voltages when clapping hands, moving arms, moving a finger, and walking were 15, 7.5, 4, and 11 V, respectively. When the hands were moved, as displayed in Figure 8C and D, voltage peaks of up to 14–15 V were recorded, as a result of the pressure imparted to the sensor site while being touched. In view of the irregularity of the forces applied, there were variations in the sizes of the voltage peaks. The PVDF/AgNP/MXene fibers exhibited exceptional stability and excellent output performance, enabling their use for energy harvesting and powering LEDs. Figure 9 reveals the ability of the sensor to power an LED through the touch of a finger.

In order to evaluate the sensing ability of the optimized PVDF/AgNP/MXene composite piezoelectric sensor, we coupled it with a circuit integrated with an Arduino microcontroller (Mega 2560). Arduino is a hardware platform used for the development of applications based on Atmel microcontrollers. The Mega 2560 model, which we applied in this study, is a standard commercial board entrusted to acquiring and recording inputs. The

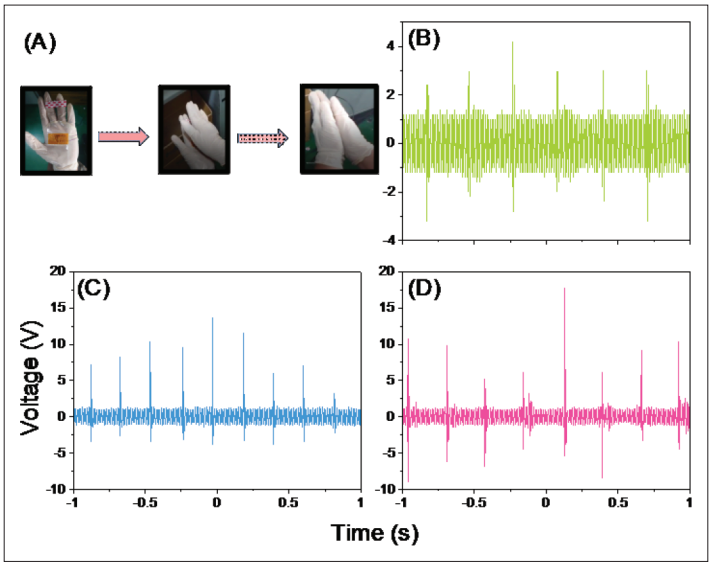


**Figure 8**. (A) Digital images of the sensor while clapping hands, and (B-D) voltage outputs of the sensor detecting the clapping of hands at various frequencies, i.e., 6, 8, and 9 Hz, respectively.

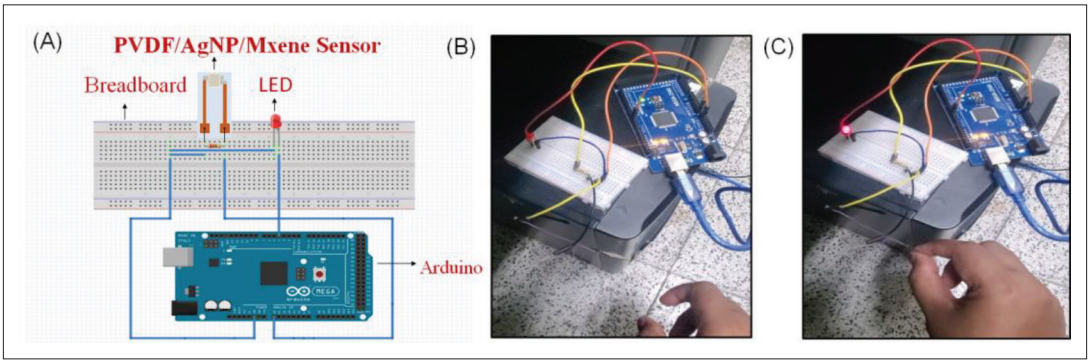


**Figure 9**. (A) Circuit schematic representation of LED which is incorporated into the circuit. (B) Image of the LED before it was lit up. (C) Image of the LED that was lit up when the sensor is touched

microcontroller was employed as an open-source electronic platform with C language programming for electrical signal processing and counting control. The voltage generated by the PVDF/AgNP/MXene composite piezoelectric sensor was used to light an LED. The Arduino, LEDs, piezoelectric sensors, and a power management circuit were placed on a breadboard to turn on the LED when the sensor was touched. Figure 9A is a schematic representation of the circuit. In this study, the positive terminal of the LED was connected to a resistor set to 1 MΩ, and it was then connected to pin4 of the Arduino, the voltage output channel of the sensor. The generated electrical voltages were further limited by a 1 MΩ resistor to protect the microcontroller from electric shocks. The LED would glow after the piezoelectric sensor had reached the threshold voltage when applying the force. Figure 9B and C reveals that a commercial red LED could indeed be lit up.

## 4. Conclusion

The addition of AgNP/MXene composite increased the electrical conductivity of PVDF, improving the piezoelectric properties of its entire fiber. FTIR spectra revealed that the contents of the α-phase of PVDF were lower, and the contents of the β-phase increased after being polarized by high electric field through NFES in PVDF as well as PVDF/AgNP, PVDF/MXene, and PVDF/AgNP/MXene composites. Electrical tapping experiments revealed that the output voltages of the energy harvester based on PVDF/AgNP/MXene composite piezoelectric fiber was higher than those of devices based on pure PVDF and PVDF/AgNP and PVDF/MXene composites, thus confirming that the addition of AgNP/MXene increased the output voltage of PVDF piezoelectric fibers. We investigated the potential use of PVDF/AgNP/MXene composite fibers as self-powered wearable sensors for the

detection of human motion, based on their exceptional flexibility and energy-harvesting capabilities. The sensor voltage outputs, depending on whether the sensor was detecting the clapping of hands or the moving of arms and fingers, ranged from 4 V to 15 V as a result of the pressure imparted to the sensor upon being touched. In view of the irregularity in the forces applied, there were variations in the sizes of the voltage peaks. The PVDF/AgNP/MXene fibers demonstrated exceptional stability and excellent output performance, enabling their use for energy harvesting and the powering of LEDs.

## Acknowledgements

The authors thank the staff at National Sun Yat-sen University for their assistance with the TEM (ID: EM022600) experiments.

## Funding

This work was supported by the grant KAFGH_A_111002 from Kaohsiung Armed Forces General Hospital and financially supported by the Ministry of Science and Technology, Taiwan, under contracts MOST 110-2124-M-002-013 and 111-2223-E-110-004.

## Conflict of interest

The authors declare no conflicts of interest.

## Author contributions

*Conceptualization:* Cheng-Tang Pan, Karishma Dutt, Amit Kumar
*Data curation:* Karishma Dutt, Rahul Kumar, Zhi-Hong Wen
*Formal analysis:* Karishma Dutt, Yi-Ting Lo
*Funding acquisitions:* Cheng-Tang Pan, Shiao-Wei Kuo
*Investigation:* Karishma Dutt, Amit Kumar
*Methodology:* Cheng-Tang Pan, Karishma Dutt
*Project administration:* Karishma Dutt
*Resources:* Cheng-Tang Pan, Shiao-Wei Ku, Cheng-Hsin Chuang
*Software:* Karishma Dutt, Chien-Shu Wang,
*Supervision:* Cheng-Tang Pan, Shiao-Wei Kuo
*Visualization:* Karishma Dutt, Shiao-Wei Kuo and
*Writing – original draft:* Karishma Dutt
*Writing – review & editing:* Cheng-Tang Pan, Karishma Dutt, Shiao-Wei Kuo

## Ethics approval and consent to participate

Not applicable.

## Consent for publication

Not applicable.

## Availability of data

Not applicable.

## References

1. Xue B, Xie H, Zhao J, *et al.*, 2022, Flexible piezoresistive pressure sensor based on electrospun rough polyurethane nanofibers film for human motion monitoring. *Nanomaterials*, 12(4): 723.

   https://doi.org/10.3390/nano12040723

2. Mohapatra Dand Subudhi B, 2022, Development of a cost effective iot-based weather monitoring system. *IEEE Consum Electron Mag*, 11: 81–86.

   https://doi.org/10.1109/MCE.2021.3136833

3. Sengupta D, Kamat AM, Smit Q, *et al.*, 2022, Piezoresistive 3D graphene-PDMS spongy pressure sensors for IoT enabled wearables and smart products. *Flex Print Electron*, 7.

   https://doi.org/10.1088/2058-8585/ac4d0e

4. Yang X, Liu G, Guo Q, *et al.*, 2022, Triboelectric sensor array for internet of things based smart traffic monitoring and management system. *Nano Energy*, 92: 106757.

   https://doi.org/10.1016/j.nanoen.2021.106757

5. Xiao P, Zhou W, Liang Y, *et al.*, 2022, Biomimetic skins enable strain-perception-strengthening soft morphing. *Adv Funct Mater*: 2201812.

   https://doi.org/10.1002/adfm.202201812

6. He J, Xiao P, Lu W, *et al.*, 2019, A Universal high accuracy wearable pulse monitoring system via high sensitivity and large linearity graphene pressure sensor. *Nano Energy*, 59: 422–433.

   https://doi.org/10.1016/j.nanoen.2019.02.036

7. He J, Xiao P, Shi J, *et al.*, 2018, High performance humidity fluctuation sensor for wearable devices via a bioinspired atomic-precise tunable graphene-polymer heterogeneous sensing junction. *Chem Mater*, 30(13): 4343–4354.

   https://doi.org/10.1021/acs.chemmater.8b01587

8. Wang S, Xiao P, Liang Y, *et al.*, 2018, Network cracks-based wearable strain sensors for subtle and large strain detection of human motions. *J Mater Chem C*, 6(19): 5140–5147.

   https://doi.org/10.1039/C8TC00433A

9. Pusty Mand Shirage PM, 2022, Insights and perspectives on graphene-PVDF based nanocomposite materials for harvesting mechanical energy. *J Alloys Compd*: 164060.

   https://doi.org/10.1016/j.jallcom.2022.164060

10. Meng K, Xiao X, Wei W, *et al.*, 2022, Wearable pressure sensors for pulse wave monitoring. *Adv Mater*, 34: e2109357.

    https://doi.org/10.1002/adma.202109357

11. Zeng X, Deng H-T, Wen D-L, *et al.*, 2022, Wearable multi-functional sensing technology for healthcare smart detection. *Micromachines*, 13(2): 254.

    https://doi.org/10.3390/mi13020254

12. Lo L-W, Zhao J, Wan H, *et al.*, 2022, A Soft sponge sensor for multimodal sensing and distinguishing of pressure, strain, and temperature. *ACS Appl Mater Interfaces*, 14(7): 9570–9578.

    https://doi.org/10.1021/acsami.1c21003

13. Dong K, Wu Z, Deng J, *et al.*, 2018, A stretchable yarn embedded triboelectric nanogenerator as electronic skin for biomechanical energy harvesting and multifunctional pressure sensing. *Adv Mater*, 30(43): 1804944.

    https://doi.org/10.1002/adma.201804944

14. Zhu M, Chng SS, Cai W, *et al.*, 2020, Piezoelectric polymer nanofibers for pressure sensors and their applications in human activity monitoring. *RSC Adv*, 10(37): 21887–21894.

    https://doi.org/10.1039/D0RA03293J

15. Hou X, Zhang S, Yu J, *et al.*, 2020, Flexible piezoelectric nanofibers/polydimethylsiloxane-based pressure sensor for self-powered human motion monitoring. *Energy Technol*, 8(3): 1901242.

    https://doi.org/10.1002/ente.201901242

16. Stadlober B, Zirkl M and Irimia-Vladu M, 2019, Route towards sustainable smart sensors: ferroelectric polyvinylidene fluoride-based materials and their integration in flexible electronics. *Chem Soc Rev*, 48(6): 1787–1825.

    https://doi.org/10.1039/C8CS00928G

17. Ribeiro C, Sencadas V, Correia DM, *et al.*, 2015, Piezoelectric polymers as biomaterials for tissue engineering applications. *Colloids Surf B*, 136: 46–55.

    https://doi.org/10.1016/j.colsurfb.2015.08.043

18. Yu G-F, Yan X, Yu M, *et al.*, 2016, Patterned, highly stretchable and conductive nanofibrous PANI/PVDF strain sensors based on electrospinning and in situ polymerization. *Nanoscale*, 8(5): 2944–2950.

    https://doi.org/10.1039/C5NR08618C

19. Zhou H, Zhang Y, Qiu Y, *et al.*, 2020, Stretchable piezoelectric energy harvesters and self-powered sensors for wearable and implantable devices. *Biosens*, 168: 112569.

    https://doi.org/10.1016/j.bios.2020.112569

20. Chorsi MT, Curry E J, Chorsi HT, *et al.*, 2019, Piezoelectric biomaterials for sensors and actuators. *Adv Mater*, 31(1): 1802084.

    https://doi.org/10.1002/adma.201802084

21. Safari Aand Akdogan E K, (eds) 2008, *Piezoelectric and acoustic materials for transducer applications*. Springer Science & Business Media, New York.

    https://doi.org/10.1007/978-0-387-76540-2

22. Cui C, Xue F, Hu W-J, *et al.*, 2018, Two-dimensional materials with piezoelectric and ferroelectric functionalities. *NPJ 2D MaterApp*, 2(1): 1–14.

    https://doi.org/10.1038/s41699-018-0063-5

23. Kapat K, Shubhra QTH, Zhou M, *et al.*, 2020, Piezoelectric nano-biomaterials for biomedicine and tissue regeneration. *Adv Funct Mater*, 30(44): 1909045.

    https://doi.org/10.1002/adfm.201909045

24. Bowen CR, Kim H A, Weaver P M, *et al.*, 2014, Piezoelectric and ferroelectric materials and structures for energy harvesting applications. *Energy Environ Sci*, 7(1): 25–44.

    https://doi.org/10.1039/C3EE42454E

25. Mias, S., & Camon, H. (2008).A review of active optical devices: II. Phase modulation. Journal of Micromechanics and Microengineering, 18(8), 083002.

    http://dx.doi.org/10.1088/0960-1317/18/8/083002

26. Tichý J, Erhart J, Kittinger E, *et al.*, 2010, *Fundamentals of piezoelectric sensorics: mechanical, dielectric, and thermodynamical properties of piezoelectric materials*. Springer Science & Business Media, London.

    https://doi.org/10.1007/978-3-540-68427-5

27. Garcia-Sanchez F, Sáez Aand Dominguez J, 2005, Anisotropic and piezoelectric materials fracture analysis by BEM. *Comput Struct*, 83(10-11): 804–820.

    https://doi.org/10.1016/j.compstruc.2004.09.010

28. Kumar D, Chaturvedi Pand Jejurikar N, 2014, Piezoelectric energy harvester design and power conditioning. *In 2014 IEEE Students' Conference on Electrical, Electronics and Computer Science*, IEEE, 1–6.

    https://doi.org/10.1109/SCEECS.2014.6804491

29. Liu Z, Li S, Zhu J, *et al.*, 2022, Fabrication of β-phase-enriched PVDF sheets for self-powered piezoelectric sensing. *ACS ApplMater Interfaces*, 14(9): 11854–11863.

    https://doi.org/10.1021/acsami.2c01611

30. Li J, Zhou G, Hong Y, *et al.*, 2022, Highly sensitive, flexible and wearable piezoelectric motion sensor based on PT promoted β-phase PVDF. *Sens Actuator A Phys*, 337: 113415.

    https://doi.org/10.1016/j.sna.2022.113415

31. Katsouras I, Asadi K, Li M, *et al.*, 2016, The negative piezoelectric effect of the ferroelectric polymer poly (vinylidene fluoride). *Nat mater*, 15(1): 78–84.

    http://dx.doi.org/10.1038/nmat4423

32. Auliya RZ, Ooi PC, Sadri R, *et al.*, 2021, Exploration of 2D Ti3C2 MXene for all solution processed piezoelectric nanogenerator applications. *Sci Rep*, 11(1): 1–13.

    https://doi.org/10.1038/s41598-021-96909-0

33. Chen J-J, Li Y, Zheng X-M, *et al.*, 2018, Enhancement in electroactive crystalline phase and dielectric performance of novel PEG-graphene/PVDF composites. *Appl Surf Sci*, 448: 320–330.

https://doi.org/10.1016/j.apsusc.2018.04.144

34. Fan FR, Tang Wand Wang ZL, 2016, Flexible nanogenerators for energy harvesting and self-powered electronics. *Adv Mater*, 28(22): 4283–4305.

https://doi.org/10.1002/adma.201504299

35. Tang C-W, Li B, Sun L, *et al.*, 2012, The effects of nanofillers, stretching and recrystallization on microstructure, phase transformation and dielectric properties in PVDF nanocomposites. *Eur Polym J*, 48(6): 1062–1072.

https://doi.org/10.1016/j.eurpolymj.2012.04.002

36. Arshad AN, Wahid MHM, Rusop M, *et al.*, 2019, Dielectric and structural properties of poly (vinylidene fluoride) (PVDF) and poly (vinylidene fluoride-trifluoroethylene) (PVDF-TrFE) filled with magnesium oxide nanofillers. *J Nanomater*, 2019.

https://doi.org/10.1155/2019/5961563

37. Jin Y, Xia Nand Gerhardt RA, 2016, Enhanced dielectric properties of polymer matrix composites with BaTiO3 and MWCNT hybrid fillers using simple phase separation. *Nano Energy*, 30: 407–416.

https://doi.org/10.1016/j.nanoen.2016.10.033

38. Lu L, Ding W, Liu J, *et al.*, 2020, Flexible PVDF based piezoelectric nanogenerators. *Nano Energy*, 78: 105251.

https://doi.org/10.1016/j.nanoen.2020.105251

39. Teo W Eand Ramakrishna S, 2006, A review on electrospinning design and nanofibre assemblies. *Nanotechnology*, 17(14): R89.

http://dx.doi.org/10.1088/0957-4484/17/14/R01

40. Liu ZH, Pan CT, Lin LW, *et al.*, 2013, Direct-write PVDF nonwoven fiber fabric energy harvesters via the hollow cylindrical near-field electrospinning process. *Smart Mater Struct*, 23(2): 025003.

http://dx.doi.org/10.1088/0964-1726/23/2/025003

41. Liu ZH, Pan CT, Lin LW, *et al.*, 2013, Piezoelectric properties of PVDF/MWCNT nanofiber using near-field electrospinning. *Sens Actuators A: Phys*, 193: 13–24.

https://doi.org/10.1016/j.sna.2013.01.007

42. Zaarour B, Zhu L, Huang C, *et al.*, 2018, Fabrication of a polyvinylidene fluoride cactus-like nanofiber through one-step electrospinning. *RSC Adv*, 8(74): 42353–42360.

https://doi.org/10.1039/C8RA09257E

43. Pan C-T, Tsai K-C, Wang S-Y, *et al.*, 2017, Development of piezoelectric fibers in smart patch by near-field electrospinning method with closed-loop motor control. *Sens Mater*, 29: 497–509.

http://dx.doi.org/10.18494/SAM.2017.1532

44. Pan C-T, Yen C-K, Wang S-Y, *et al.*, 2015, Near-field electrospinning enhances the energy harvesting of hollow PVDF piezoelectric fibers. *RSC Adv*, 5(103): 85073–85081.

https://doi.org/10.1039/C5RA16604G

45. Pan C-T, Yen C-K, Wu H-C, *et al.*, 2015, Significant piezoelectric and energy harvesting enhancement of poly (vinylidene fluoride)/polypeptide fiber composites prepared through near-field electrospinning. *J Mater Chem A*, 3(13): 6835–6843.

https://doi.org/10.1039/C5TA00147A

46. Pan C-T, Yen C-K, Wang S-Y, *et al.*, 2018, Energy harvester and cell proliferation from biocompatible PMLG nanofibers prepared using near-field electrospinning and electrospray technology. *J Nanosci Nanotechnol*, 18(1): 156–164.

https://doi.org/10.1166/jnn.2018.14596

47. Takamatsu S, Takahata T, Muraki M, *et al.*, 2010, Transparent conductive-polymer strain sensors for touch input sheets of flexible displays. *J MicromechMicroeng*, 20(7): 075017.

http://dx.doi.org/10.1088/0960-1317/20/7/075017

48. Zou J, Yip H-L, Hau SK, *et al.*, 2010, Metal grid/conducting polymer hybrid transparent electrode for inverted polymer solar cells. *Appl phys lett*, 96(20): 96.

https://doi.org/10.1063/1.3394679

49. Emmott CJM, Urbina Aand Nelson J, 2012, Environmental and economic assessment of ITO-free electrodes for organic solar cells. *Sol Energy Mater Sol Cells*, 97: 14–21.

https://doi.org/10.1016/j.solmat.2011.09.024

50. Wu C Mand Chou MH, 2016, Polymorphism, piezoelectricity and sound absorption of electrospun PVDF membranes with and without carbon nanotubes. *Compos scitechnol*, 127: 127–133.

https://doi.org/10.1016/j.compscitech.2016.03.001

51. Sun J-G, Yang T-N, Wang C-Y, *et al.*, 2018, A flexible transparent one-structure tribo-piezo-pyroelectric hybrid energy generator based on bio-inspired silver nanowires network for biomechanical energy harvesting and physiological monitoring. *Nano Energy*, 48: 383–390.

https://doi.org/10.1016/j.nanoen.2018.03.071

52. Pusty M, Sinha Land Shirage PM, 2019, A flexible self-poled piezoelectric nanogenerator based on a rGO–Ag/PVDF nanocomposite. *New J Chem*, 43(1): 284–294.

https://doi.org/10.1039/C8NJ04751K

53. Abolhasani MM, Shirvanimoghaddam Kand Naebe M, 2017, PVDF/graphene composite nanofibers with enhanced

piezoelectric performance for development of robust nanogenerators. *Compos Sci Technol*, 138: 49–56.

https://doi.org/10.1016/j.compscitech.2016.11.017

54. Afroj S, Tan S, Abdelkader AM, *et al.*, 2020, Highly conductive, scalable, and machine washable graphene-based E-textiles for multifunctional wearable electronic applications. *Adv Funct Mater*, 30(23): 2000293.

https://doi.org/10.1002/adfm.202000293

55. Ren M, Zhou Y, Wang Y, *et al.*, 2019, Highly stretchable and durable strain sensor based on carbon nanotubes decorated thermoplastic polyurethane fibrous network with aligned wave-like structure. *Chem Eng J*, 360: 762–777.

https://doi.org/10.1016/j.cej.2018.12.025

56. Wu L, Wang L, Guo Z, *et al.*, 2019, Durable and multifunctional superhydrophobic coatings with excellent joule heating and electromagnetic interference shielding performance for flexible sensing electronics. *ACS Appl Mater Interfaces*, 11(37): 34338–34347.

https://doi.org/10.1021/acsami.9b11895

57. Seyedin S, Uzun S, Levitt A, *et al.*, 2020, MXene composite and coaxial fibers with high stretchability and conductivity for wearable strain sensing textiles. *Adv Funct Mater*, 30(12): 1910504.

https://doi.org/10.1002/adfm.201910504

58. Park H, Brown PR, Bulović V, *et al.*, 2012, Graphene as transparent conducting electrodes in organic photovoltaics: studies in graphene morphology, hole transporting layers, and counter electrodes. *Nano Lett*, 12(1): 133–140.

https://doi.org/10.1021/nl2029859

59. Araki T, Jiu J, Nogi M, *et al.*, 2014, Low haze transparent electrodes and highly conducting air dried films with ultra-long silver nanowires synthesized by one-step polyol method. *Nano Res*, 7(2): 236–245.

https://doi.org/10.1007/s12274-013-0391-x

60. Pan C-T, Yen C-K, Lin L, *et al.*, 2014, Energy harvesting with piezoelectric poly (γ-benzyl-l-glutamate) fibers prepared through cylindrical near-field electrospinning. *RSC Adv*, 4(41): 21563–21570.

https://doi.org/10.1039/C4RA01452A

61. Kim GH, Hong S Mand Seo Y, 2009, Piezoelectric properties of poly (vinylidene fluoride) and carbon nanotube blends: β-phase development. *Phys Chem Chem Phys*, 11(44): 10506–10512.

https://doi.org/10.1039/B912801H

62. Wu C Mand Chou MH, 2020, Acoustic-electric conversion and piezoelectric properties of electrospun polyvinylidene fluoride/silver nanofibrous membranes. *Express Polym Lett*, 14(2): 103–114.

https://doi.org/10.3144/expresspolymlett.2020.10

63. Nthunya LN, Derese S, Gutierrez L, *et al.*, 2019, Green synthesis of silver nanoparticles using one-pot and microwave-assisted methods and their subsequent embedment on PVDF nanofibre membranes for growth inhibition of mesophilic and thermophilic bacteria. *New J Chem* 43(10): 4168–4180.

https://doi.org/10.1039/C8NJ06160B

64. Laroche G, Lafrance CP, Prud'homme RE, *et al.*, 1998, Identification and quantification of the crystalline structures of poly (vinylidene fluoride) sutures by wide-angle X-ray scattering and differential scanning calorimetry. *JBMRA*, 39(2): 184–189.

https://doi.org/10.1002/(SICI)1097-4636(199802)39:2%3C184::AID JBM3%3E3.0.CO;2-L

65. Issa AA, Al-Maadeed MA, Luyt AS, *et al.*, 2017, Physico-mechanical, dielectric, and piezoelectric properties of PVDF electrospun mats containing silver nanoparticles. *C*, 3(4): 30.

https://doi.org/10.3390/c3040030

66. Lou X, Chen J, Xiong Z, *et al.*, 2021, Porosity design on conjugated microporous poly (aniline) S for exceptional mercury (II) removal. *ACS Appl Mater Interfaces*, 13: 51.

https://doi.org/10.1016/j.compscitech.2020.108360

67. Samy MM, Mohamed M Gand Kuo S-W, 2020, Pyrene-functionalized tetraphenylethylene polybenzoxazine for dispersing single-walled carbon nanotubes and energy storage. *Compos Sci Technol*, 199: 108360.

https://doi.org/10.1016/j.compscitech.2020.108360

68. Mohamed MG, Samy MM, Mansoure T H, *et al.*, 2022, Dispersions of 1, 3, 4-oxadiazole-linked conjugated microporous polymers with carbon nanotubes as a high-performance electrode for supercapacitors. *ACS Appl Energy Mater*, 5(3): 3677–3688.

https://doi.org/10.1021/acsaem.2c00100

69. Lu F-H, Chang F-C, Mohamed M-G, *et al.*, 2014, Conducting Ag/oligothiophene complex pastes through a simple quenching/chelation method. *J Mater Chem C*, 2(30): 6111–6118.

https://doi.org/10.1039/C4TC00731J

70. Wang H, Wu Y, Zhang J, *et al.*, 2015, Enhancement of the electrical properties of MXene Ti3C2 nanosheets by post-treatments of alkalization and calcination. *Mater Lett*, 160: 537–540.

https://doi.org/10.1016/j.matlet.2015.08.046

71. Huang X, Wu P, 2020, A facile, high-yield, and freeze-and-thaw-assisted approach to fabricate MXene with plentiful wrinkles and its application in on-chip micro-supercapacitors. *Adv Funct Mater*, 30(12): 1910048.

https://doi.org/10.1002/adfm.201910048

72. Cai Y, Shen J, Ge G, *et al.*, 2018, Stretchable Ti3C2T x MXene/carbon nanotube composite based strain sensor with ultrahigh sensitivity and tunable sensing range. *ACS Nano*, 12(1): 56–62.

https://doi.org/10.1021/acsnano.7b06251

73. Mirkhani SA, Shayesteh Zeraati A, Aliabadian E, *et al.*, 2019, High dielectric constant and low dielectric loss via poly (vinyl alcohol)/Ti3C2T x MXene nanocomposites. *ACS Appl Mater Interfaces*, 11(20): 18599–18608.

https://doi.org/10.1021/acsami.9b00393

74. Xia Y, Mathis TS, Zhao M-Q, *et al.*, 2018, Thickness-independent capacitance of vertically aligned liquid-crystalline MXenes. *Nature*, 557(7705): 409–412.

https://doi.org/10.1038/s41586-018-0109-z

75. Ran J, Gao G, Li F-T, *et al.*, 2017, Ti3C2 MXene co-catalyst on metal sulfide photo-absorbers for enhanced visible-light photocatalytic hydrogen production. *Nat commun*, 8(1): 1–10.

https://doi.org/10.1038/ncomms13907

76. Liu LX, Chen W, Zhang HB, *et al.*, 2019, Flexible and multifunctional silk textiles with biomimetic leaf-like MXene/silver nanowire nanostructures for electromagnetic interference shielding, humidity monitoring, and self-derived hydrophobicity. *Adv Funct Mater*, 29(44): 1905197.

https://doi.org/10.1002/adfm.201905197

77. Zhao X, Wang L-Y, Tang C-Y, *et al.*, 2020, Smart Ti3C2T x MXene fabric with fast humidity response and joule heating for healthcare and medical therapy applications. *ACS Nano*, 14(7): 8793–8805.

https://doi.org/10.1021/acsnano.0c03391

78. Yue Y, Liu N, Liu W, *et al.*, 2018, 3D hybrid porous Mxene-sponge network and its application in piezoresistive sensor. *Nano Energy*, 50: 79–87.

https://doi.org/10.1016/j.nanoen.2018.05.020

79. Feng Y, Deng Q, Peng C, *et al.*, 2018, An ultrahigh discharged energy density achieved in an inhomogeneous PVDF dielectric composite filled with 2D MXene nanosheets via interface engineering. *J Mater Chem C*, 6(48): 13283–13292.

https://doi.org/10.1039/C8TC05180A

80. Feng Y, Deng Q, Peng C, *et al.*, 2019, High dielectric and breakdown properties achieved in ternary BaTiO3/MXene/PVDF nanocomposites with low-concentration fillers from enhanced interface polarization. *Ceram Int*, 45(6): 7923–7930.

https://doi.org/10.1016/j.ceramint.2019.01.104

81. Tu S, Jiang Q, Zhang X, *et al.*, 2018, Large dielectric constant enhancement in MXene percolative polymer composites. *ACS nano*, 12(4): 3369–3377.

https://doi.org/10.1021/acsnano.7b08895

82. Zhao Q, Yang L, Ma Y, *et al.*, 2021, Highly sensitive, reliable and flexible pressure sensor based on piezoelectric PVDF hybrid film using MXene nanosheet reinforcement. *J Alloys Compd*, 886: 161069.

https://doi.org/10.1016/j.jallcom.2021.161069

83. Wang S, Shao H-Q, Liu Y, *et al.*, 2021, Boosting piezoelectric response of PVDF-TrFE via MXene for self-powered linear pressure sensor. *Compos Sci Technol*, 202: 108600.

https://doi.org/10.1016/j.compscitech.2020.108600

84. Fan X, Ding Y, Liu Y, *et al.*, 2019, Plasmonic Ti3C2T x MXene enables highly efficient photothermal conversion for healable and transparent wearable device. *ACS nano*, 13(7): 8124–8134.

https://doi.org/10.1021/acsnano.9b03161

85. Zhai W, Wang C, Wang S, *et al.*, 2021, Ultra-stretchable and multifunctional wearable electronics for superior electromagnetic interference shielding, electrical therapy and biomotion monitoring. *J Mater Chem A*, 9(11): 7238–7247.

https://doi.org/10.1039/D0TA10991F

86. Saidi A, Gauvin C, Ladhari S, *et al.*, 2021, Advanced functional materials for intelligent thermoregulation in personal protective equipment. *Polymers*, 13(21): 3711.

https://doi.org/10.3390/polym13213711

87. Rana SMS, Rahman MT, Salauddin M, *et al.*, 2021, Electrospun PVDF-TrFE/MXene nanofiber mat-based triboelectric nanogenerator for smart home appliances. *ACS Appl Mater Interfaces*, 13(4): 4955–4967.

https://doi.org/10.1021/acsami.0c17512

88. Kim J, Jang M, Jeong G, *et al.*, 2021, MXene-enhanced β-phase crystallization in ferroelectric porous composites for highly-sensitive dynamic force sensors. *Nano Energy*, 89: 106409.

https://doi.org/10.1016/j.nanoen.2021.106409

89. Pan C-T, Dutt K, Yen C-K, *et al.*, 2022, Characterization of piezoelectric properties of Ag-NPs doped PVDF nanocomposite fibres membrane prepared by near field electrospinning. *Comb Chem High Throughput Screen*, 25(4): 720–729.

https://doi.org/10.2174/1386207324666210302100728

90. Yen C-K, Dutt K, Yao Y-S, *et al.*, 2022, Development of flexible biceps tremors sensing chip of PVDF fibers with nano-silver particles by near-field electrospinning. *Polymers*, 14(2): 331.

https://doi.org/10.3390/polym14020331

91. Chen W-w, An Z-l, He L-b, *et al.*, 2015, Piezoelectric coefficients measurement for PVDF films with pneumatic pressure rig in a sole cavity. *In 2015 Symposium on Piezoelectricity, Acoustic Waves, and Device Applications (SPAWDA)*, IEEE, 111–114.

https://doi.org/10.1109/SPAWDA.2015.7364452

92. Huang Z, Zhang Q, Corkovic S, *et al.*, 2006, Comparative measurements of piezoelectric coefficient of PZT films by berlincourt, interferometer, and vibrometer methods. *IEEE Trans Ultrason Ferroelectr Freq Control*, 53(12): 2287–2293.

https://doi.org/10.1109/TUFFC.2006.175

93. Chang C, Tran VH, Wang J, *et al.*, 2010, Direct-write piezoelectric polymeric nanogenerator with high energy conversion efficiency. *Nano Lett*, 10(2): 726–731.

https://doi.org/10.1021/nl9040719

94. Yen CK, Tsao CH, Pan CT, *et al.*, 2014, Electrospun PVDF fibers on bio-wings using multi-spinnerets. *In The 9th IEEE International Conference on Nano/Micro Engineered and Molecular Systems (NEMS)*, IEEE, 609–613.

https://doi.org/10.1109/NEMS.2014.6908885

95. Fu J, Hou Y, Zheng M, *et al.*, 2020, Flexible piezoelectric energy harvester with extremely high power generation capability by sandwich structure design strategy. *ACS Appl Mater Interfaces*, 12(8): 9766–9774.

https://doi.org/10.1021/acsami.9b21201

96. Singh HH, Singh Sand Khare N, 2018, Enhanced β-phase in PVDF polymer nanocomposite and its application for nanogenerator. *Polym Adv Technol*, 29(1): 143–150.

https://doi.org/10.1002/pat.4096

97. Shepelin NA, Sherrell PC, Skountzos EN, *et al.*, 2021, Interfacial piezoelectric polarization locking in printable Ti3C2Tx MXene-fluoropolymer composites. *Nat commun*, 12(1): 1–11.

https://doi.org/10.1038/s41467-021-23341-3

98. Jiang Z, Tan X, Huang Y, 2022, Piezoelectric effect enhanced photocatalysis in environmental remediation: State-of-the-art techniques and future scenarios. *Sci Total Environ*, 806: 150924.

https://doi.org/10.1016/j.scitotenv.2021.150924

99. Pan C-T, Tsai K-C, Wang S-Y, *et al.*, 2017, Large-area piezoelectric PVDF fibers fabricated by near-field electrospinning with multi-spinneret structures. *Micromachines*, 8(4): 97.

https://doi.org/10.3390/mi8040097